Author(s): Ruokola, Päivi; Dadu, Elina; Kazmertsuk, Artur; Häkkänen, Heikki; Marjomäki, Varpu; Ihalainen, Janne

Title: Raman Spectroscopic Signatures of Echovirus 1 Uncoating

Year: 2014

Version:

Please cite the original version:

Ruokola, P., Dadu, E., Kazmertsuk, A., Häkkänen, H., Marjomäki, V., & Ihalainen, J. (2014). Raman Spectroscopic Signatures of Echovirus 1 Uncoating. Journal of Virology, 88(15), 8504-8513. https://doi.org/10.1128/JVI.03398-13

Raman spectroscopic signatures of echovirus 1 uncoating

Päivi Ruokola[†], Elina Dadu[†], Artur Kazmertsuk[†],

Heikki Häkkänen[†], Varpu Marjomäki[†] and Janne A. Ihalainen[†,≠]

[†]Nanoscience Center, Department of Biological and Environmental Science, University of Jyväskylä, P.O Box 35, FI-40014 Jyväskylä, Finland

[≠] To whom correspondence should be addressed. E-mail: janne.ihalainen@jyu.fi.

ABSTRACT

During the last decades Raman spectroscopy has entered the biological and medical fields. It enables non-destructive analysis of structural details at molecular level, and has been used to study viruses and their constituents. Here we use Raman spectroscopy to study echovirus 1 (EV1), a small, non-enveloped human pathogen, in two different uncoating states induced by heat treatments. Raman signals of capsid proteins and RNA genome were observed from the intact virus, uncoating intermediate, and disrupted state. Transmission electron microscopy data revealed general structural changes between the studied particles. Compared to the intact virion, the spectral characteristics of the proteins of the heat-treated particles indicated reducing α-helix content with respect to β-sheets and coil structures. Changes observed in tryptophan and tyrosine signals suggest an increasingly hydrophilic environment around these residues. RNA signals revealed a change in the environment of the genome, and in its conformation. The ionized carbonyl vibrations showed small changes between the intact virion and the disrupted particles, which points out to cleavage of salt bridges in the protein structure during the uncoating process. In conclusion, our data reveals distinguishable Raman signatures of the intact, intermediate, and disrupted EV1 particles. These changes indicate structural, chemical and solute-solvent alterations in the genome and in the capsid proteins and lay the essential ground work for investigating the uncoating of EV1 and related viruses in real time.

IMPORTANCE

In order to combat against virus infection we need to know the details of virus uncoating. We present here the novel Raman signatures for opened and intact

Echovirus 1. This gives hope that the signatures may be used in the near future to evaluate the ambient conditions in endosomes leading to virus uncoating using e.g. CARS imaging. These studies will complement well the structural studies on virus uncoating. In addition, Raman/CARS imaging offers possibility for dynamic live measurements in vitro and in cells which are impossible for example by cryo electron tomography. Furthermore, as viral Raman spectra can be overwhelmed with various contaminants, we find our study being extremely up-to date to demonstrate the importance of the sample preparation for Raman spectroscopy in the field of virology.

INTRODUCTION

Picornaviruses are small, non-enveloped human pathogens able to cause a wide range of illnesses (1). The subgroup enteroviruses include clinically important echoviruses, coxackieviruses and poliovirus. These viruses cause a variety of symptoms varying from mild infections to aseptic meningitis, heart muscle damage and paralysis. Enteroviruses have also recently been associated with chronic diseases such as type 1 diabetes, cardiomyopathies and atherosclerosis (2,3). Structural details of these viruses have been obtained by means of x-ray crystallography or at a lower resolution by cryo-electron microscopy (4). Various imaging techniques together with biochemical analysis have revealed important information about their entry to cells and the subsequent events leading to the uncoating and virus replication (5,6). However, information available on the physico-chemical details of genome release events of enteroviral particles is sparse. The uncoating process has been extensively studied by initiating the genome release using heat treatments where intact virions are irreversibly converted to subviral

particles that resemble naturally occurring uncoating intermediates (7,8,9). Recently, using such temperature manipulated particles; a long-standing paradigm of the genome release model from the 5-fold axis has been revised (10, 11). Yet, at the present, the biochemical events leading to the genome release as well as the initiating environmental trigger of uncoating is missing (1). Further studies are thus important for addressing one of the events in the enteroviral life cycle, the genome release, and also for the possibility of spotting new potential antiviral targets against related enteroviruses.

Echovirus 1 (EV1) is a picornavirus belonging to a structurally related group of enteroviruses. Common to all picornaviruses, EV1 is icosahedron-shaped (T=1) assembly of 60 copies of identical protomers comprised of four viral proteins (VP1, VP2, VP3 and VP4), which encapsulate a positive-sense single-stranded RNA genome of approximately 7500 nucleotides. A 14-carbon saturated fatty acid, myristate, is covalently attached to the N-terminus of each picornavirus VP4 capsid protein (12), and it is thought to exit the capsid simultaneously with VP4 during the uncoating process (13). Additionally, studies on poliovirus have shown that the N-terminus of VP1 is externalized to the virion surface during the uncoating process increasing the overall hydrophobicity of the particle (14). Also, the release of the stability-mediating pocket factor, characterized as palmitic acid and located in the core of VP1, is thought to be a prerequisite in the uncoating process, as was shown for bovine enterovirus (15,16).

Raman spectroscopy provides specific signatures of proteins, nucleic acids and lipids. It can reveal vast amount of information about changes taking place in the

chemical content of the particles, in the protein secondary structure and in the physical environment of the particles, which undergo biologically important transformations (17). Raman spectroscopy is a noninvasive characterization technique, which uses visible light laser beams, and thus enables microscopic mode with the same resolution as in fluorescence microscopy. As the acquisition can be fast, processes in real time can be studied. As Raman spectra are only slightly disturbed by water environment, information of molecules in their natural habitat or under a wide range of conditions can be obtained. This makes it an ideal probe to study detailed structural alterations, viral protein assembly, interactions, and dynamics, without any labels or other invasive sample preparation methods.

Raman spectroscopic studies on viruses, such as Turnip Yellow Mosaic Virus (TYMV) (18), Bean Pod Mottle Virus (BPMV) (19,20), Belladonna Mottle Virus (BDMV) (21) and bacteriophages, such as filamentous bacteriophage Ff (22,23), PRD1 virus (24) and P22 (25-27) have been reported. However, these viruses differ substantially from enteroviruses in several aspects. In the case of plant viruses, TYMV, BPMV and BDMV, the genome is bound to the protein capsid in static form, whereas in the enteroviruses the interior of the virion is spatially disordered with respect to the symmetric protein shell (28). In addition, the subunit packing is somewhat different between these bromoviruses and enteroviruses (28). The bacteriophage PRD1 is icosahedral in shape, but has a lipid envelope. P22 phage is non-enveloped, head-tail structured virus, with 6 prominent tail spikes. All such properties influence the Raman spectroscopic character of these viruses.

Detailed Raman spectroscopic signatures from the virus uncoating process of

enteroviruses, both *in vivo* and *in vitro*, are missing. For such studies linear Raman experiments of the initial and final states are a prerequisite. Here, we characterize vibrational spectroscopic properties of intact EV1 virions and investigate the spectral differences arising in the uncoating process of EV1 particles *in vitro.* We elucidate, first of all, the Raman spectroscopic basis of recognition between the intact virion and the disrupted EV1 particle. Further, we show Raman signature of the uncoating intermediate, which is obtained by heating the intact, infectious particles at 50°C. Previous studies utilizing heat treatments in order to produce and to investigate uncoating intermediates of enteroviruses have produced a wealth of information. Heating enterovirus particles at 50-60°C for varying amount of time has been shown to be able to produce uncoating intermediate (135S), genome ejecting as well as empty (80S) particles indistinguishable from those observed *in vivo* (7,10,11). The Raman spectra of the particles heat-treated at 50°C represent a state where the genome is partially ejected from the capsid, as confirmed by transmission electron microscopy (TEM) and thermal stability assay (29). We conclude that there are clear Raman markers, which address the uncoating stage of the virion. The experiments reported here provide a framework for monitoring the sequence of chemical and conformational changes occurring during enterovirus uncoating in a time-resolved manner.

MATERIALS AND METHODS

Cell culture and virus purification

Echovirus 1 (Farouk strain, obtained from ATCC) was propagated in a monolayer of GMK cells and purified using similar overall scheme as described in Ref. (30). To

146 summarize, overnight (24 h) infected cells were collected and repeatedly
147 freeze/thawed (3 cycles) to lyse cellular structures. Bulk cell debris was removed by
148 centrifugation (4500 x g for 15 min). To precipitate protein, 8% (w/v) PEG-6000
149 (Sigma-Aldrich) and 2.2% (w/v) NaCl were added to the supernatant and stirred
150 overnight (24h) at 4°C. Precipitated material was collected by centrifugation (8000 x
151 g for 40 min) and suspended in R-buffer (10 mM Tris-HCl, pH 7.5, 200 mM NaCl, 50
152 mM $MgCl_2$, 10% (w/v) glycerol). To disrupt membranous structures, 0.3% (w/v) of
153 sodium deoxycholate (Sigma-Aldrich) and 0.6% (v/v) of Nonident^{TM} P 40 substitute
154 (Sigma-Aldrich) were added to the suspension and incubated for 30 min at 4°C. The
155 resulting mixture was clarified by centrifugation (3500 x g for 15 min) and divided
156 equally (<1.5 ml/gradient) on top of 10 ml linear density gradients of 10 to 40% (w/v)
157 sucrose in R-buffer. The gradients were subsequently ultra-centrifuged (86 000 x g
158 for 3 h at 4°C) and fractioned from the top into 500 µl aliquots. Based on optical
159 density measurement at 260 nm (NanoDrop 1000, Thermo scientific), three virion
160 containing fractions (#11, #12 and #13) were pooled and diluted to 10 ml in PBS
161 supplemented with 2 mM $MgCl_2$. The diluted fractions were dialyzed thrice against 1
162 L of PBS supplemented with 2 mM $MgCl_2$ using 50 kDa Molecular weight cut-off
163 Spectra/Por® Float-A-Lyzer® Cellulose Ester membrane (Spectrum laboratories).
164 Finally, dialyzed virions were pelleted by ultracentrifugation (93000 x g for 2 h at 4°C)
165 and suspended in a small volume of PBS supplemented with 2 mM $MgCl_2$. All
166 measured samples were dissolved in the aforementioned PBS buffer. Virions were
167 stored at -80°C.
168
169 **Infectivity of the purified EV1 virions**
170 Infectivity of the purified virus batch was assayed using end-point-titration method to

171 determine 50% Tissue Culture Infective Dose ($TCID_{50}$). The $TCID_{50}$ value was
172 calculated as described in Ref. (31) positioning the $TCID_{50}$ value between the last
173 infected and first non-infected well. Briefly, a monolayer of GMK cells seeded at
174 $5*10^4$ ml^{-1} on a 96-well plate were infected with serially diluted virus stock (starting
175 from 10^{-5} dilution). The progression of the infection was followed daily by light
176 microscope. After 72 h incubation period the cells were stained using crystal violet
177 supplemented with 10% formalin (for 10 min at RT). The detached cells were
178 washed away with water and remaining attached cells were counted as viable and
179 non-infected. For the EV1 batches used in the experiments, the $TCID_{50}$/ml was found
180 to be $6.1*10^{11}$-$1.5*10^{12}$.
181
182 **Protein content and composition of purified EV1**
183 Protein content of the purified EV1 was determined using a method described by
184 Porterfield et al. (32) where an average value of VP1-4 molecular mass (23.5 kDa)
185 and an average value of VP1-4 molar absorptivity (ε_{280} 34440 M^{-1} cm^{-1}) were used
186 for the calculations. Protein concentrations of the batches were 0.9 - 3.8 mg ml^{-1}
187 after subtracting scattering component (6.9% of the baseline subtracted absorption
188 signal at 260 nm). The 260/280 ratio was 1.65. Absorption spectrum was recorded
189 with PerkinElmer Lambda 850 spectrophotometer using 10.0 mm optical path quartz
190 cuvette (Hellma Analytics). The protein composition of purified EV1 was analyzed
191 using 12% SDS-PAGE. Sample lane was loaded with 5 µg of EV1 and PageRuler^{TM}
192 Plus (Thermo Scientific) was used as a molecular weight marker.
193
194 **Thermal stability**
195 Thermal stability of the purified EV1 particles was assayed using method described

196 by Walter et al (29). Fluorescence signal was recorded using Bio-Rad C1000 thermal
197 cycler, and the final sample mixture contained 1 µg of EV1 and 10X concentration of
198 SYBR® Green II (Invitrogen). All samples were equilibrated at 20°C for 10 min before
199 starting thermal stability measurements. For the full temperature range scan the
200 fluorescence signal was recorded at 10 s intervals with 0.5°C increments. In
201 additional measurements, the designated temperature was kept constant for 3
202 minutes (50°C) or 10 minutes (60°C), and after heat treatment the sample was
203 cooled back to 20°C at which point the fluorescence reading was taken or loaded to
204 EM grid.
205
206 **Transmission electron microscopy**
207 Morphology of the heated and non-heated virions was visualized by negative
208 staining with 1% (w/v) phosphotungstic acid (Sigma-Aldrich). The formvar-coated EM
209 grids were glow-discharged (EMS/SC7620 Mini Sputter Coater) and samples were
210 deposited on the grids for 15 seconds after which the excess sample was blotted
211 away (Whatman 3MM). Next, negative stain was added for 1 minute and removed as
212 before. Samples dried for at least overnight were imaged with JEM-1400 (JEOL)
213 transmission electron microscope with 50 000 x magnification (80 kV).
214
215 **Raman spectroscopy**
216 For all Raman viral experiments, aliquots of 6-10 µl with sample concentration 0.9
217 mg ml^{-1} for dried samples and 3.8 mg ml^{-1} for aqueous samples were deposited
218 either on a CaF_2-window, or sealed in a glass capillary (American Dade SMI
219 Capillaries: P5070-902). Heating of the aqueous samples was performed in a water
220 bath, either at 50°C for 3 min or at 60°C for 10 min. The dried sample was allowed to

221 dry for 15 min at ambient temperature. The Raman spectra were measured with a
222 home built Raman setup in a backscattering geometry. In this setup a laser beam of
223 solid-state laser (CNI) with excitation wavelength at 532 nm was focused onto the
224 sample with a spot diameter of 3 μm using a microscope objective (Zeiss, Plan-
225 NEOFLUAR 10x/0.30). Raman scattering was recorded using a CCD camera
226 (Andor, Newton DU940P-BV) attached to an imaging spectrograph (Acton Spectra
227 Pro 2500i) with entrance slit of 50 μm and grating of 600 grooves/mm. Raman
228 spectra were accumulated using 30 x 10 s exposures. Laser power of 45 mW for
229 dried and 200 mW for aqueous samples was used. From each scan a dark spectrum
230 was subtracted. The reference spectra of water, buffer solution, empty capillary, and
231 CaF_2 -window were detected with the same settings and subtracted from the sample
232 spectra. The fluorescence background was defined by fitting a polynomial curve to
233 the measured spectrum from the points where no Raman signal is expected to be
234 present, and subtracted from the data. After this procedure, no other spectral
235 signatures than viral constituents were obtained.
236
237 Spectra of the aqueous samples of concentration 3.8 mg ml^{-1} represent mean values
238 of measurements from three different EV1 batches normalized to the Phe peak at
239 1003 cm^{-1} with a floating average with a span of three data points (2.7 cm^{-1}). In
240 addition, the differences between room temperature and heated samples were
241 analyzed in four separated spectral sections, 610-945 cm^{-1}, 945-1145 cm^{-1}, 1145-
242 1520 cm^{-1}, and 1520-1800 cm^{-1}, which were normalized to the mean signals of each
243 section and smoothed with a floating average with a span of seven data points (10
244 cm^{-1}).
245

Radial distribution and positioning of salt bridges in EV1

The atom coordinates were gathered from EV1 protomer (PDB entry: 1EV1) using UCFS Chimera (33) build 1.8. Salt bridges were identified manually scoring only arginine and lysine as salt bridge forming residues with carboxylic oxygen of Glu and Asp. In case of many possible connections (<3.5 Å) the closest was chosen resulting in one connection per residue.

RESULTS

Sample purity and heat-induced uncoating of EV1

The Raman analysis of viral particles imposes a demand for highly homogenous and pure samples. The sucrose gradient purification scheme used here resulted in a single clearly visible band. The fractioned gradient showed a local absorbance maximum at 260 nm in fraction 12, while five top fractions also showed high optical density; no visible banding was observed (Fig. 1A). After dialysis the collected fractions (Fr#11-13) were analyzed for protein composition using 12% SDS-PAGE. Fig. 1C shows that the purified EV1 was contaminant-free in the molecular weight range of 250-10 kDa, while the prominent capsid proteins, VP1-3, banded next to 35-25 kDa markers, as expected. To quantify the protein concentration of a virus sample, a UV-Vis spectroscopic method introduced by Porterfield et al. (32) was used. In our hands, the above-mentioned spectroscopic approach has been found to be in a reasonable agreement with the more traditional Bradford assay (data not shown). The method incorporates scattering correction in the resulting absorption spectrum, with 6.9% of the total signal. This subsequently affects the 260/280 ratio, which was 1.65 for dialyzed particles (Fig. 1B). In literature, the reported 260/280

ratios for enteroviruses vary considerably (34-36), partially due to differences in genome contents, but also resulting from uncorrected spectra. However, as the genome to protein ratio (260/280) does not reflect virion integrity, EV1 was visualized by TEM and was found to consist of a highly homogenous population of intact particles approximately 25 nm in diameter (Fig. 1D).

Since the EV1 capsid proved to be non-permeable to the SYBR Green II dye (Fig. 2A), thermal stability assay was used along with TEM to evaluate the extent of genome egress from intact EV1 particles. Fig. 2A indicates the melting temperature (T_m) for intact EV1 particles to be 51°C. Noting that the increase in SYBR Green II signal begins to rise around 40°C and accumulates approximately 3 minutes of effective heating time prior to the 51°C T_m mark, 3 minute heating at 50°C was used to produce the so-called uncoating intermediate particles (Fig. 2B). The population of these genome-releasing virions was visualized by TEM (Fig. 3). After 3 minutes of heating at 50°C great majority of the visualized particles were connected to a protruding density (Fig. 3B). Additionally, Figs. 3A and 3B show both the intact (20°C) virions and partially disrupted virions (50°C) to be structurally organized and symmetrical in shape. Similar particles have been obtained earlier using polioviruses (11). Heating the intact EV1 virions at 60°C resulted in a complete particle disruption (Fig. 3C). Over all, homogenously genome deprived but structurally intact EV1 particles were challenging to produce by heat treatment alone (data not shown). The heat-induced chemical and structural alterations in the particles treated at 20°C, 50°C and 60°C temperatures were then further probed by Raman spectroscopy.

Raman analysis of viral particles

296 The Raman spectrum of the intact virion (Fig. 4) shows a large amount of vibrations
297 that can be assigned reasonably well using literature values as expressed in Tables
298 1A and 1B, for proteins and RNA, respectively (17,24,37,38,39). The most prominent
299 vibrational region is the aliphatic C-H stretching complex shown at around 2900
300 cm^{-1}. Here we concentrate, however, to the fingerprint region from 600 to 1800 cm^{-1},
301 where most previous biological applications of Raman spectroscopy have been
302 performed, as it has higher sensitivity to structural and chemical nature of particles
303 (see e.g. 18,23). The best known spectral features found at typical positions (17) in
304 the Raman spectra of the virus are Am I and Am III bands at around 1670 cm^{-1} and
305 in the region between 1230 and 1300 cm^{-1}, respectively. The anti-symmetric C-C
306 stretching modes of aromatic amino acids (Phe, Tyr, and Trp) locate in the region of
307 1580-1615 cm^{-1} and the ring breathing modes of aromatic amino acids at around
308 1000 cm^{-1}. Other side-chain vibrations emerge at around 600-900 cm^{-1}, and the
309 methyl/methylene vibration bands locate at around 1350 and 1450 cm^{-1}. Many RNA
310 vibrations partially overlap with the protein bands, although a large amount of
311 vibrations can still be specified. The ring breathing modes of RNA bases appear in
312 the region below 800 cm^{-1}, ribose and phosphate signals between 800 and 1100 cm^{-1}
313 , and the stretching vibrations of the bases at higher wavenumbers (1200-1600 cm^{-1}
314) (39,40).
315
316 Raman spectra of viral particles in buffer environment show clear similarities with
317 spectra of the dried particles (Fig. 4B) and basically all spectral features can be
318 observed from the solution with concentration as low as 0.9 mg ml^{-1}. The details of
319 the spectra are, however, more clearly distinguished from the noise-level of our
320 experiment at virus concentration of 3.8 mg ml^{-1}, which is, thus, used in the

characterization of the heat-induced changes of the viral particles.

By detecting Raman spectra of the particles treated with different temperatures we aimed to indicate chemical and structural changes between the intact virus particles and an uncoating intermediate virion particle, as well as with an end-point structure where the virion particle was disrupted by heat treatment (morphology of particles obtained with TEM (vide supra, Fig. 3)). As shown in Fig. 5, the Raman spectra of the particles heat-treated at 50°C and 60°C deviate clearly from that of the intact virion. As the heat treatment changes the form (Fig. 3) and possibly also the solvent shell of the particles, the scattering and fluorescence properties of the particles differ. This creates challenges in baseline determination and normalization of the spectra, and due to this the Raman spectra were dissected in four individual spectral regions from 610 to 1800 cm^{-1}. Figs. 5A-D show the differences between the particles. In most cases, a gradual change of Raman spectra from intact to 50°C treated, and then to 60°C treated particles, is observed. This effect can be expected according to the TEM analysis as well (Fig. 3), which shows basically a full disruption of the particles after 60°C heat treatment.

The largest changes in the spectra are observed in signals assigned to the Amide bands, methyl/methylene signal at 1446 cm^{-1}, and RNA signals at 750-800 cm^{-1}, although many changes locate in regions where multiple factors affect to the spectra. Interestingly, the 1446 cm^{-1} band, reflecting C-H vibrations from the proteins, is more affected than the corresponding band for RNA molecules at 1478 cm^{-1}. Thus, the ratio between 1446 and 1478 cm^{-1} conveniently indicates changes of signals between proteins and genome, respectively, in the viral particles. The Am I and Am

III regions, shown in Fig. 5, reveal information on the changes in the secondary structure of the coat proteins in the heat-treated particles. The differences between the spectra are the most pronounced at 1630-1650 cm^{-1} and 1670 cm^{-1} (Fig. 5D). Broadening of the Am I peak is largest in the spectrum of the intact virus. On the lower energy side of Am I vibration, the 1575 cm^{-1} band, which originates from ring breathing modes, both from Trp as well as from adenine and guanine of RNA (39,41), shows higher intensity in the heated particles, especially in the spectra of the particles treated at 60°C.

Most of the heat-induced changes grow gradually as the heat-treatment becomes more intensive. Some of the changes, however, are only evident after heat treatment at 50°C, namely, the decrease of signals at 990 and 1650 cm^{-1}. These changes locate at sites where both RNA and protein vibrations attribute to the signals. At around 990 cm^{-1}, there are RNA vibrations from ribose phosphate (39), and protein derived signals from proline, arginine and tyrosine residues, as well as the nearby phenyl alanine signal at 1003 cm^{-1} (37). At 1650 cm^{-1} the signal originates from the amide bonds of proteins (17).

Apart from major differences in the Raman signals, subtle signal variations along the spectra can reveal information from important details of the EV1 uncoating process. These changes along with the assignments are indicated in Tables 1A and 1B. For example, a slight change in the signal at around 1710 cm^{-1} in the spectra of the particles treated at 50°C can be observed (Fig. 5D). This signal increase could imply protonation changes of carboxylic groups of Glu residues (42). In ideal case, such increase of signal of the protonated forms of Glu should lead to decrease of signals

371 of COO^- population, found from region between 1390 cm^{-1} and 1410 cm^{-1}, which,
372 however, is hard to detect in Fig. 5C from spectrum of viruses heat-treated at 50°C.
373 Another small change, a shift to lower wavenumbers, or decrease of signal at the
374 higher frequency side of the band, is seen in the peak at 1122-1128 cm^{-1} (Fig. 5B).
375 This peak represents non-aromatic amino acid residues, but it might also include
376 some fatty acid vibrations. There are two kinds of fatty acids in EV1 capsid, myristate
377 and palmitic acids, the first covalently attached to VP4 and the second buried in VP1
378 formed pocket. No obvious fatty acid peaks can be detected from the spectra, but
379 there are small decreases in signals of heat-treated viruses at the fatty acid signal
380 sites at 1063 cm^{-1}, 1129 cm^{-1}, and 1296 cm^{-1} (37), that could be consistent with heat-
381 induced changes in the local environment of the fatty acid molecules, or reduction of
382 fatty acid molecule amounts at the measured spot of the sample.
383
384 The Fermi doublets of the aromatic amino acids Trp and Tyr are often used as
385 indicators of indole environment hydrophobicity and phenolic hydrogen bonding.
386 Neither Fermi doublet stands out very clearly from the spectra, but can be assigned
387 to specific signals none the less. Small changes are seen in signals assigned for the
388 Tyr Fermi doublet at 829 and 854 cm^{-1} (Fig. 5A), where heat treatments reduce the
389 ratio I_{829}/I_{854}, indicative of a greater hydrogen bond acceptor role, or exposure to the
390 solvent, of the average phenoxyl group after heat treatments (43). The Trp Fermi
391 doublet at 1340 and 1360 cm^{-1} shows a small increase in the signal at 1340 cm^{-1}
392 after heat treatment (Fig. 5C), indicating an increasingly hydrophilic environment of
393 Trp residues (44,45), although the overlapping RNA signal assigned to the larger
394 peak at 1335 cm^{-1} might affect this as well. Trp band at around 880 cm^{-1} has been
395 considered a marker for Trp hydrogen bonding, with signals at 882-883 cm^{-1}

indicating Trp residues with no hydrogen bonding, and at 871 cm^{-1} with strong hydrogen bonding (44). In intact viruses this Trp signal is a single peak centered at 877 cm^{-1}, and after heat treatments the signal divides to two peaks at 873 and 881 cm^{-1}, indicating changes in Trp hydrogen bonding status. The frequency of the Trp signal near 1550 cm^{-1} has been reported to be indicative of changes in side chain conformation (46-48), and there are heat-induced changes in this region in our data (Fig. 5D). Particularly, in the spectrum of the intact virus this signal overlaps with the peak at 1572 cm^{-1}, and after heat treatment there appears a new peak slightly under 1550 cm^{-1}, suggesting a considerable change in conformation of some of the Trp residues. Similar change has been noticed with Bovine enterovirus uncoating with resonance Raman spectroscopy (46). However, also RNA signal appears relatively close at around 1578 cm^{-1}. Yet another Trp peak, at 756 cm^{-1}, also shows apparent heat-induced changes, complementing the interpretation that Trp residues undergo significant changes upon virus uncoating.

Partially overlapping with the Trp 756 cm^{-1} signal is an RNA signal at 783 cm^{-1}, coming from the C/U ring breathing modes (Fig. 5A). This signal has been reported to change in intensity due to changes in the environment, particularly in non-helical regions of RNA (39,49). In our experiment, there are heat-induced changes around this peak. A small increase is also seen in the symmetric phosphate streching vibration signal at 811 cm^{-1}, considered a marker for A form RNA helix, suggesting a change in RNA backbone conformation. Most of the RNA signals somewhat overlap with protein signals - however, RNA can be considered to be the main source of the peaks at 1335 and 1478 cm^{-1}. More detailed assignments of signals to RNA vibrations are expressed in Table 1B (39). Most RNA assigned signals above 1200

421 cm^{-1} slightly increase in intensity after heat-treatments, with one exception. The
422 decrease at 1300 cm^{-1} could come from changes in cytosine or adenine ring
423 stretching vibrations, although it could also be due to fatty acids or changes in
424 protein secondary structures. A signal just below 1050 cm^{-1}, that can be assigned to
425 RNA P-O and sugar phosphate -C-O- stretching, only appears after heat-treatments.
426

427 ## DISCUSSION

428

429 Virus particles of various species or in different assembling or uncoating states
430 deviate from each other in terms of structure and chemical content. In this study,
431 EV1 viral particles, in three different states, are characterized both in terms of
432 structural and chemical information. The intact virion, the uncoating intermediate
433 produced after heating the virion at 50°C for 3 min, and the disrupted viral particle
434 treated at 60°C for 10 min, all showed different types of structures obtained by TEM
435 analysis. Also, the Raman spectroscopy of different states produced unique spectral
436 features.
437

438 The Raman spectrum of a complex biological sample is a mixture of spectral
439 contributions from all Raman active molecular groups contained in the sample, and
440 therefore it enables studying simultaneously all sections taking part in the biological
441 processes and ultimately determining the sequence of the changes taking place in
442 the molecule. As a result, the Raman spectrum of a virus consists of numerous,
443 overlapping bands and peak shoulders. The most prominent spectral features, seen
444 in the spectra of large polypeptides, are Am I originating from the polypeptide chain
445 C=O stretching, and Am III, mainly resulting from the coupled C-N and N-H bending

446 motions. These are widely used as indicators of the secondary structure of proteins
447 (17). Other informative Raman marker bands originate from the aromatic amino
448 acids. Although Raman spectra of biological material are usually interpreted mainly
449 as indicators of secondary structure conformation, other factors in the local
450 environment influence strongly to the position, size, and shape of the Raman signal.
451 Local electric fields, polarity and protonation state of the vibrators (50) play an
452 important role, which means that Raman signals are sensitive to ions, charged
453 amino acids, and even charged phosphates in the protein or in the genome. As
454 shown in this and other studies (18-20,22-27), Raman spectroscopy can provide vast
455 amount of information about the character and status of virion particles. In many
456 cases, however, all information is difficult to distil out from a single set of data. In the
457 following we will condense the essential features of the Raman fingerprint of EV1
458 and discuss some of the crucial factors needed to consider when striving for the
459 genuine Raman spectra from viral samples in aqueous environment.
460
461 As Raman signals are relatively weak, in comparison with for example fluorescence
462 signals of fluorophores, relatively high sample concentrations are needed. Typically,
463 the reported Raman spectra of viral particles are measured with concentrations up to
464 80-100 mg ml^{-1} (18-27). Low sample concentrations are favorable when aiming to
465 measure the viral particles in non-aggregated form. On many occasions the
466 scattering intensity of viruses is small, and the changes at low concentrations are
467 hidden inside the overruling background spectra. This leads to challenges in
468 detecting the Raman signal of the sample and accurately subtracting the solvent and
469 other background from the weak viral spectra (41). It is also important to keep in
470 mind that some buffers include groups that have similar vibrations as many biological

samples, or in the worst case are quite reactive (51), and therefore can – if not obscure the spectra, at least skew the interpretation. Other informative vibrations may be deluged in a heterogeneous sample containing leftovers, such as sugars, from the purification procedure. The material besides the sample may then result in the biggest changes in the Raman spectra, overlapping the small changes taking place in the actual sample. Alternatively they may influence the behavior of the sample, for example sucrose is known to stabilize protein structure (52). In our measurements, the viral particles were clearly dominated by sucrose contamination even after dialysis with 2 kDa molecular weight cut off (data not shown), and were properly purified only with higher molecular weight cut off of 50 kDa. Also, in a recently published article of virus-like particles, there are clear - yet identified - sucrose leftovers in the Raman spectra (53). It is important to notice that because Raman spectroscopy “sees everything”, the purity and homogeneity of the samples is crucial. Even smallest changes in the purification method used can cause additions and interference to the spectra, which can lead to erroneous interpretation. This means the purification procedure must be paid critical attention to, and, as a result, better quality spectra containing more information are achieved. Further, once a spectrum of a pure viral sample has been obtained, Raman spectroscopy could be used as a very sensitive probe for impurity studies for analytical purposes.

To the best of our knowledge, there are no previous Raman studies on EV1 and its close relatives. Bovine enterovirus and rhinovirus have been studied by means of surface enhanced Raman scattering (SERS) and ultraviolet resonance Raman spectroscopy (54,55). Notable is that, in the case of SERS, the choice of the substrate material, and in the case of resonance Raman studies, the choice of the

laser wavelength, all contribute to the intensity of each Raman transition. Our spectra of EV1 are similar especially to those obtained for the BPMV virion (20), which shares considerable structural similarity with picornaviruses (56). Li et al also observed differences in the Raman spectra between crystalline and liquid BPMV viral particles, and concluded changes mainly originating from the packed RNA molecules having different electrostatic environments in the samples (57). It should be recognized, though, that one particular difference with most of the previously reported linear Raman data is that our Raman spectra have been measured with much lower protein concentrations, in our study being under 4 mg ml^{-1} versus the 80 mg ml^{-1} or more in other studies (see e.g. 19,20,24). The amount of aggregation and interaction between viral particles at such concentrations could diminish the differences compared to the crystalline state. In our EV1 samples there are differences between spectra measured in solvated and dried states, for example a broadening or a shift in Am I band to higher wavenumbers, indicating a higher amount of disordered secondary structures in the dried sample. On the other hand, the width of some bands originating from individual amino acids, like the Phe band at 1003 cm^{-1}, show similar width in spectra of dried and solvated samples. Drying removes the stabilizing hydration shell (58) and can influence the stability, cause aggregation, and hamper at least certain parts of capsid structures. This also implies that the SERS technique (55), where viral particles are attached to metallic surface or nanoparticles, can reveal somewhat different vibrational spectroscopic information than when measuring viral particles normally diffusing freely in a buffer solution.

Care was taken to remove contribution of the wagging mode of water molecules from the Raman data of the diluted samples, which has been addressed to be essential

521 for a proper analysis of the Am I modes (41). The Raman Am I band centered at
522 1668 cm^{-1} indicates β-sheets as the predominant secondary structure of the capsid,
523 which is consistent with the known structure of the major capsid proteins, VP1, VP2
524 and VP3 in EV1 (59). Temperature induced alterations around 1653 cm^{-1} reveal,
525 however, a decrease in α-helical secondary structure due to the partial unfolding of
526 the shell subunits especially at the intermediate state. The decreasing signal in Am
527 III area at around 1300 cm^{-1} could also be due to reduced α-helical content of
528 proteins. This indicates that the heat-induced uncoating is dominating in the α-helical
529 regions of the protein. The signals assigned to β-sheets and coiled structures in Am I
530 and III regions, at 1668 and 1240 cm^{-1}, respectively, are at the same time increasing
531 in magnitude, suggesting that some of the α-helix structures are converted to β-
532 sheets or coils. Flexible loops between structured domains are known to make
533 protein dynamics less constrained, and serve a critical role in the uncoating process.
534 For example, these mechanically uncoupled structures could enable the capsid
535 expansion, which is clearly visible from the TEM-image of the uncoated EV1 particle
536 (Fig. 3C).
537
538 Signals of aromatic amino acids reveal information on hydrogen bonding,
539 hydrophobicity, and side chain conformation of these residues (43-48). Many of
540 these informative signals of EV1 change with heat treatments. Small changes are
541 seen in the Fermi doublets of Tyr and Trp that change with hydrogen bonding of Tyr
542 and hydrophobicity of Trp environment. Changes in the 877 cm^{-1} signal indicate
543 variation in Trp hydrogen bonding status, and the appearance of a new Trp signal at
544 around 1550 cm^{-1} indicates changes in side chain conformations. All these signals
545 point to the same direction as the changes seen in secondary structures of viral

546 proteins and TEM-images, i.e. loosening of the capsid structure and subsequent
547 exposure of these residues to water.
548
549 Obtaining Glu vibrations of protonated carboxyl group suggests protonation
550 processes to take place in the heat-induced uncoating of EV1. In the unprotonated
551 state, the negatively charged Glu may interact with positively charged residues (e.g.
552 Lys, Arg) to form salt bridges, which have been shown to be important stabilizers of
553 HIV, influence virus, filamentous viruses, and Bacteriophage hk97 (60-63). These
554 salt bridges may be involved in constrained network of interactions within one
555 subunit or between two neighboring units, clamping the domains in a considerably
556 more stable capsid structure. Our data suggest that salt bridges may be involved in
557 fine-tuning the metastable capsid structure of EV1. By studying the EV1 structure,
558 the distribution of possible salt bridges in the EV1 structure were shown to reside in
559 the interior of the capsid or buried within the capsid structure (Figs. 6A,B).
560 Interestingly, the enterovirus uncoating intermediates reported are shown to have
561 lost the internal protein VP4 (13), which mediates two inter-protomer and one inter-
562 VP salt bridge connection (Fig. 6C). It is thus tempting to speculate that, at least
563 partially, the extraction of VP4 from the capsid particle might be controlled by salt
564 bridges. In comparison to the native virion, the heat-induced uncoating intermediate
565 of EV1 showed a small increase in the protonated carboxylic acid stretching. Also, a
566 small decrease in signals that could be assigned to fatty acids was detected. The
567 disconnected salt bridges, together with the expelled fatty acid chains, are expected
568 to shift the capsid dynamics into a more flexible motion as these constrains are
569 removed.
570

In addition to the changes in the capsid proteins, several heat-induced changes in the RNA signals were observed. In general, the changes are difficult to interpret as particular structural changes, but more like a general change of the solute-solvent interactions of the RNA molecule. Especially, the signal variation at 783 cm^{-1} suggests that there are changes in the RNA solvation shell (39,49). Both the ejection of genome and an increased permeability of the capsid structure could explain these changes in the signal sensitive to the environment of RNA. Still, also a small increase in the A form helix marker band at 811 cm^{-1} (39,40) after heat treatment at 60°C suggests that RNA is no longer bound by the intact capsid structure and refolds to the A form double helical structure.

In conclusion, we were able to acquire signature Raman spectra that distinguish between the intact and uncoated EV1 diluted in buffer at relatively low concentrations. Very little vibrational spectroscopic data exists of the conformational changes during the viral uncoating so far. The observed Raman signatures are in good agreement with the present knowledge of enteroviral uncoating. For example, the UV-resonance Raman study comparing the intact and empty bovine enterovirus particles (46) revealed increasing hydrophobicity of the virus, or moving of Trp residues to increasingly hydrophilic environment during the viral opening process, consistent with our measurements. However, the detected differences between the intact virion in dried phase and in the liquid state indicate that the natural environment is essential in order to retain all the information from the uncoating process. Most biological macromolecules are physiologically active in aqueous solutions, and water molecules are supposed to play a crucial role in the function and structure of biomolecules.

596

597 The Raman signatures of EV1 virion particles consist of numerous signals, the most
598 pronounced features being 1) Amide bands: The Am I became less broad after the
599 uncoating process and revealed a decrease of α-helical structures and an increase
600 of irregular structures or β-sheets, 2) Aromatic amino acids: The vibration modes of
601 tryptophan and tyrosine residues suggest loosening of the capsid structure with
602 increasing hydrophilicity around these residues, 3) Chemical changes in the virion
603 particles: The carbonyl vibrations showed small changes between the native virion
604 and the heated particles, which indicates at least partial disruption of salt bridges, 4)
605 Genome signals: RNA signatures indicate both changes in the environment of the
606 genome, and a change in RNA conformation.

607

608 The observed differences in the Raman spectra between the intact and uncoated
609 virions give novel insight into the structural changes occurring during virus opening.
610 Most probably the findings are similar for the enteroviruses that are close relatives to
611 EV1. The prominent Raman marker bands of the intact virion, intermediate uncoating
612 state of the virion, and disrupted virion particle represented here also enable *in vivo*
613 studies of factors leading to viral uncoating in cellular structures with Raman
614 mapping and coherent anti-Stokes Raman Scattering microscopy.

615

616 ACKNOWLEDGEMENTS

617

618 This research is supported by the Academy of Finland (134061 and 257125) and the
619 National Doctoral Programme in Nanoscience (NGS). The authors wish to thank Alli
620 Liukkonen, Eila Korhonen, and Arja Mansikkaviita for practical help, together with

Tommi Isoniemi for supportive studies. Prof. Dr Thomas Huser, Prof. Dr Mika Pettersson, Dr. Olli Pentikäinen and Vesa Aho are warmly appreciated for valuable discussions.

REFERENCES

1. **Tuthill TJ, Groppelli E, Hogle JM, Rowlands DJ.** 2010. Picornaviruses. Curr Top Microbiol Immunol. **343**: 43–89

2. **Hober D, Sauter P.** 2011. Pathogenesis of type 1 diabetes mellitus: interplay between enterovirus and host. Nat. Rev. Endocrinol. **6**: 279-289

3. **Roivainen M, Alfthan G, Jousilahti P, Kimpimaki M, Hovi T, Tuomilehto J.** 1998 Enterovirus infections as a possible risk factor for myocardial infarction. Circulation. **98**: 2534-2537

4. **Fry EE, Stuart DI.** 2010. Virion structure. In the Picornaviruses. Ehrenfeld E, Domingo E, Roos RP, editors. ASM Press/Washington, USA. 59–71

5. **Brandenburg B, Lee LY, Lakadamyali M, Rust MJ, Zhuang X, Hogle JM.** 2007. Imaging poliovirus entry in live cells. PLOS Biology. **5**: 1543-1555

6. **Karjalainen M, Rintanen N, Lehkonen M, Kallio K, Mäki A, Hellström K, Siljamäki V, Upla P, Marjomäki V.** 2011. Echovirus 1 infection depends on biogenesis of novel multivesicular bodies. Cellular Microbiology. **13**: 1975-1995

7. **Curry S, Chow M, Hogle JM.** 1996. The poliovirus 135S particle is infectious. J Virol. **70**: 7125–7131

8. **Bubeck D, Filman DJ, Cheng N, Steven AC, Hogle JM, Belnap DM.** 2005. The structure of the poliovirus 135S cell entry intermediate at 10-angstrom resolution

645 reveals the location of an externalized polypeptide that binds to membranes. J. Virol.
646 **79**: 7745-55
647 9. **Lin J, Cheng N, Chow M, Filman DJ, Steven AC, Hogle JM, Belnap DM.** 2011.
648 An externalized polypeptide partitions between two distinct sites on genome-
649 released poliovirus particles. J. Virol. **85**: 9974-83
650 10. **Levy HC, Bostina M, Filman DJ, Hogle JM.** 2010. Catching a Virus in the Act of
651 RNA Release: a Novel Poliovirus Uncoating Intermediate Characterized by Cryo-
652 Electron Microscopy. J. Virol. **84**: 4426–4441
653 11. **Bostina M, Levy H, Filman DJ, Hogle JM.** 2011. Poliovirus RNA is released
654 from the capsid near a twofold symmetry axis. J. Virol. **85**: 776-783
655 12. **Chow M, Newman JFE, Filman D, Hogle JM, Rowlands DJ, Brown F.** 1987.
656 Myristylation of picornavirus capsid protein VP4 and its structural significance.
657 Nature. **327**: 482-86
658 13. **Fricks CE, Hogle JM.** 1990. Cell-Induced conformational change in poliovirus:
659 Externalization of the amino terminus of VP1 is responsible for liposome binding. J.
660 Virology. **64**: 1934-1945
661 14. **Racaniello VR.** 1996. Early events in poliovirus infection: Virus-receptor
662 interactions. Proc. Natl. Sci. USA. **93**: 11378-11381
663 15. **Smyth M, Pettitt T, Symonds A, Martin J.** 2003. Identification of the pocket
664 factors in a picornavirus. Arch Virol. **148**: 1225–1233
665 16. **Smyth MS, Martin JH.** 2002. Picornavirus uncoating. J Clin Pathol: Mol Pathol.
666 **55**: 214–219
667 17. **Tuma R.** 2005. Raman spectroscopy of proteins: from peptides to large
668 assemblies. J. Raman Spectrosc. **36**: 307-319
669 18. **Hartman KA, McDonald-Ordzie PE, Kaper JM, Prescott B, Thomas GJ Jr.**

1978. Studies of virus structure by laser-Raman spectroscopy. Turnip yellow mosaic virus and capsids. Biochemistry. **17**: 2118-23

19. **Li TS, Johnson JE, Thomas GJ Jr.** 1992. Raman dynamic probe of hydrogen exchange in bean pod mottle virus: base-specific retardation of exchange in packaged ssRNA. Biochemistry. **31**: 6673-6682

20. **Li TS, Chen ZG, Johnson JE, Thomas GJ Jr.** 1990. Structural studies of bean pod mottle virus, capsid, and RNA in crystal and solution states by laser Raman spectroscopy. Biochemistry. **29**: 5018-5026

21. **Prescott B, Sitaraman K, Argos P, Thomas GJ Jr.** 1985. Protein-RNA interactions in belladonna mottle virus investigated by laser Raman spectroscopy. Biochemistry. **24**: 1226-1231

22. **Overman SA, Aubrey KL, Vispo NS, Cesareni G, Thomas GJ Jr.** 1994. Novel tyrosine markers in Raman spectra of wild-type and mutant (Y21M and Y24M) Ff virions indicate unusual environments for coat protein phenoxyls. Biochemistry. **33**: 1037-1042

23. **Overman SA, Thomas GJ Jr.** 1995. Raman spectroscopy of the filamentous virus Ff (fd, fl, M13): structural interpretation for coat protein aromatics. Biochemistry. **34**: 5440-5451

24. **Tuma R, Bamford J, Bamford D, Russell M, Thomas GJ Jr.** 1996. Structure, interactions and dynamics of PRD1 Virus II. Organization of the viral membrane and DNA. J. Mol. Biol. **257**: 102-115

25. **Fish SR, Hartman KA, Fuller MT, King J, Thomas GJ.** 1980. Investigation of secondary structures and macromolecular interactions in bacteriophage p22 by laser Raman spectroscopy. Biophys J. **32**: 234-327

26. **Aubrey KL, Casjens SR, Thomas GJ Jr.** 1992. Secondary structure and

695 interactions of the packaged dsDNA genome of bacteriophage P22 investigated by
696 Raman difference spectroscopy. Biochemistry. **31**: 11835–11842
697 27. **Reilly KE, Thomas GJ Jr.** 1994. Hydrogen exchange dynamics of the P22 virion
698 determined by time-resolved Raman spectroscopy. Effects of chromosome
699 packaging on the kinetics of nucleotide exchanges. J. Mol. Biol. **241**: 68–82
700 28. **Hogle JM, Chow M, Filman DJ.** 1985. Three-dimensional structure of poliovirus
701 at 2.9 Å resolution. Science. **229**: 1358-1365
702 29. **Walter TS, Ren J, Tuthill TJ, Rowlands DJ, Stuart DI, Fry EE.** 2012. A plate-
703 based high-throughput assay for virus stability and vaccine formulation. J. Virol
704 Methods.**185**: 166-170
705 30. **Abraham G, Colonno RJ.** 1984. Many rhinovirus stereotypes share the same
706 cellular receptor. J. Virology. **51**: 340-345
707 31. **Reed LJ, Muench H.** 1938. A simple method of estimating fifty percent
708 endpoints. Am. J. Hyg. **27**: 493–497
709 32. **Porterfield JZ, Zlotnick A.** 2010. A simple and general method for determining
710 the protein and nucleic acid content of viruses by UV absorbance. Virology. **407**:
711 281-288
712 33. **Pettersen EF, Goddard TD, Huang CC, Couch GS, Greenblatt DM, Meng EC,**
713 **Ferrin TE.** 2004. UCSF Chimera--a visualization system for exploratory research
714 and analysis J. Comput. Chem. **13**: 1605-1612
715 34. **McGregor S, Mayer HD.** 1968. Biophysical studies on rhinovirus and poliovirus.
716 I. Morphology of viral ribonucleoprotein. J. Virol. **2**: 149-154
717 35. **Ren J, Wang X, Hu Z, Gao Q, Sun Y, Li X, Porta C, Walter TS, Gilbert RJ,**
718 **Zhao Y, Axford D, Williams M, McAuley K, Rowlands DJ, Yin W, Wang J, Stuart**
719 **DI, Rao Z, Fry EE.** 2013. Picornavirus uncoating intermediate captured in atomic

720 detail. Nat. Commun. **4**: 1929

721 36. **Wang X, Peng W, Ren J, Hu Z, Xu J, Lou Z, Li X, Yin W, Shen X, Porta C,**
722 **Walter TS, Evans G, Axford D, Owen R, Rowlands DJ, Wang J, Stuart DI, Fry**
723 **EE, Rao Z.** 2012. A sensor-adaptor mechanism for enterovirus uncoating from
724 structures of EV71. Nat. Struct. Mol. Biol. **19**: 424-429

725 37. **De Gleder J, De Gussem K, Vandenabeele P, Moens L.** 2007. Reference
726 database of Raman spectra of biological molecules. J. Raman Spectrosc. **38**: 1133-
727 1147

728 38. **Matthäus C, Bird B, Miljkovic M, Chernenko T, Romeo M, Diem M.** 2008.
729 Infrared and Raman microscopy in cell biology. Methods in Cell Biology. **89**: 275-308

730 39. **Hobro AJ.;, Rouhi M, Blanch EW, Conn GL.** 2007 Raman and Raman optical
731 activity (ROA) analysis of RNA structural motifs in Domain I of the EMCV IRES.
732 Nucleic Acids Research **35**: 1169-1177

733 40. **Hobro AJ, Standley DM, Ahmad S, Smith NI.** 2013. Deconstructing RNA:
734 optical measurement of composition and structure. Phys.Chem.Chem.Phys. **15**:
735 13199-13208

736 41. **Sane SA, Cramer SM, Przybycien TM.** 1999. A holistic approach to protein
737 secondary structure characterization using amide I band Raman Spectroscopy. Anal.
738 Biochemistry. **269**: 255-272

739 42. **Barth A, Zscherp C.** 2002. What vibrations tell about proteins. Q.Rev.Biophys.
740 **35**: 369-430

741 43. **Siamwiza MN, Lord RC, Chen MC, Takamatsu T, Harada I, Matsuura H,**
742 **Shimanouchi T.** 1975. Interpretation of the doublet at 850 and 830 cm-1 in the
743 Raman spectra of tyrosyl residues in proteins and certain model compounds.
744 Biochemistry. **14**: 4870-6

745 44. **Miura T, Takeuchi H, Harada I.** 1988. Characterization of individual tryptophan
746 side chains in proteins using Raman spectroscopy and hydrogen-deuterium
747 exchange kinetics. Biochemistry. **27**: 88-94
748 45. **Schlamadinger DE, Gable JE, Kim JE.** 2009. Hydrogen Bonding and Solvent
749 Polarity Markers in the UV Resonance Raman Spectrum of Tryptophan: Application
750 to Membrane Proteins. J Phys Chem B. **113**: 14769-14778
751 46. **Kaminaka S, Imamura Y, Shingu M, Kitagawa T, Toyoda T.** 1999. Studies of
752 bovine enterovirus structure by ultraviolet resonance Raman spectroscopy. J. Virol.
753 Methods. **77**: 117-123
754 47. **Miura T, Takeuchi H, Harada I.** 1989. Tryptophan Raman bands sensitive to
755 hydrogen bonding and side-chain conformation. J.Raman Spectrosc. **20**: 667-671
756 48. **Takeuchi H.** 2003. Raman structural markers of tryptophan and histidine side
757 chains in proteins. Biopolymers. **72**: 305-317
758 49. **Hernández B, Baumruk V, Leulliot N, Gouyette C, Huynh-Dinh T, Ghomi M.**
759 2003. Thermodynamic and structural features of ultrastable DNA and RNA hairpins.
760 J.Mol.Struct. **651–653**: 67-74
761 50. **Park ES, Boxer SG.** 2002. Origins of the sensitivity of molecular vibrations to
762 electric fields: carbonyl and nitrosyl stretches in model compounds and proteins. J.
763 Phys. Chem. B. **106**: 5800-5806
764 51. **Taha M, Ming-Jer L.** 2010. Interactions of TRIS
765 [tris(hydroxymethyl)aminomethane] and related buffers with peptide backbone:
766 Thermodynamic characterization. Chem. Phys. **12**: 12840–12850
767 52. **Allison SD, Dong A, Carpenter JF.** 1996. Counteracting effects of thiocyanate
768 and sucrose on chymotrypsinogen secondary structure and aggregation during
769 freezing, drying, and rehydration. Biophys. J. **71**: 2022-2032

770 53. **Lu X, Liu Q, Benavides-Montano JA, Nicola AV, Aston DE, Rasco BA,**
771 **Aguilar HC.** 2013. Detection of receptor-induced glycoprotein conformational
772 changes on enveloped virions by using confocal micro-Raman spectroscopy. J. Virol.
773 **87**: 3130-3142
774 54. **Shanmukh S, Jones L, Driskell J, Zhao Y, Dluhy R, Tripp RA.** 2006. Rapid
775 and sensitive detection of respiratory virus molecular signatures using a silver
776 nanorod array SERS substrate. Nano letters. **6**: 2630-2636
777 55. **Joisson C, Kuster F, Plaué S, Van Regenmortel MH.** 1993. Antigenic analysis
778 of bean pod mottle virus using linear and cyclized synthetic peptides. Arch Virol. 128:
779 299-317
780 56. **Li TS, Chen ZG, Johnson JE, Thomas GJ Jr.** 1992. Conformations,
781 interactions, and thermostabilities of RNA and proteins in bean pod mottle virus:
782 investigation of solution and crystal structures by laser Raman spectroscopy.
783 Biochemistry. **31**: 6673-6682
784 57. **Prestrelski SJ, Tedeschi N, Arakawa T, Carpenter JF.** 1993. Dehydration-
785 induced conformational transitions in proteins and their inhibition by stabilizers.
786 Biophys J. **65**: 661-71
787 58. **Filman DJ, Wien MW, Cunningham JA, Bergelson JM, Hogle JM.** 1998.
788 Structure determination of Echovirus 1. Acta Cryst. **54**: 1261-1272
789 59. **He Y, Liu S, Li J, Lu H, Qi Z, Liu Z, Debnath AK, Jiang S.** 2008. Conserved
790 salt bridge between the N- and C-terminal heptad repeat regions of the human
791 immunodeficiency virus type 1 gp41 core structure is critical for virus entry and
792 inhibition. J. Virol. **82**: 11129-11139
793 60. **Rachakonda PS, Veit M, Korte T, Ludwig K, Böttcher C, Huang Q, Schmidt**
794 **MF, Herrmann A.** 2007. The relevance of salt bridges for the stability of the influenza

795 virus hemagglutinin. FASEB J. **21**: 995-1002
796 61. **Dolja VV, Boyko VP, Agranovsky AA, Koonin EV.** 1991. Phylogeny of capsid
797 proteins of rod-shaped and filamentous RNA plant viruses: two families with distinct
798 patterns of sequence and probably structure conservation. Virology. **184**: 79-86
799 62. **Gertsman I, Fu CY, Huang R, Komives EA, Johnson JE.** 2010. Critical salt
800 bridges guide capsid assembly, stability, and maturation behavior in bacteriophage
801 HK97. Mol. Cell. Proteomics. **9**: 1752-1763
802 63. **Wu H, Volponi JV, Oliver AE, Parikh AN, Simmons BA, Singh S.** 2011. In vivo
803 lipidomics using single-cell Raman spectroscopy. Proc.Natl.Acad.Sci.U.S.A. **108**:
804 3809-3814
805
806
807
808
809
810
811

812 Table 1. A collection of obtained frequencies of the vibrations, together with their

813 assignments, based on previous studies (17,24,37,38,39).

814

815

TABLE 1A A collection of obtained frequencies of the vibrations of proteins found in this study. The assignment is based on the previous studies (17,24,37,38).

Assignment	Dried sample, frequency, cm^{-1}	Aqueous sample, frequency, cm^{-1}	Heat-induced effect
Phe	623	620	+
Tyr	644	642	
C-S	670	668	
Trp	758	756	+
Tyr	826,855	829,854	-(829)/+(854)
Trp	887	873-883	- (60°C)
AmIII,	960-978	952-977	
Phe	1003	1003	
Phe	1031	1031	
CC, CH	1071-1096	1073-1098	+
non-aromatic side chains	1127	1122-1128	+(1120)/-(1130)
CH_3	1156-1176	1160-1178	
Phe, Tyr	1208	1205-1210	
Am III	1230-1300	1230-1300	+(1240)/-(1300)
Trp, CH3	1318-1378	1322-1383	
Asp, Glu -COO^-	1390-1404	1390-1402	+ (60°C)
CH_2	1446-1458	1446-1458	-
Trp	1555,1573	1549,1572	+
Phe		1588-1594	-
Phe, Trp	1605	1603	
Tyr, Trp	1613,1618	1612,1616	
Am I	1669	1668	+
Asp, Glu -COOH		1710	+ (50°C)
Abbreviations: Am, amide.			

816

817

818

TABLE 1B A collection of obtained frequencies assigned to the RNA molecule from the intact virus particles. The assignment is based on the study of Hobro et al (39).			
Assignment	Dried sample, frequency, cm^{-1}	Aqueus sample, frequency, cm^{-1}	Heat-induced effect
A ring stretching (726)	726	722-727	
C/U breathing/stretching (787)	783	783	changes
O-P-O symmetric stretching (813)	811	811	+ (60°C)
Ribose-Phosphate,-C-O-stretching (919)		914-921	-
Ribose-Phosphate,-C-O-stretching (977)		969-980	-
P-O stretch, sugar phosphate –C-O- stretching (1047)	1044	1044sh	+
PO_2^- symmetric stretch (1097)	1091-1100	1090-1100	
U/C ring stretching (1253)	1252	1250	
C/A ring stretching (1300)	1300	1300	-
A,G,U (1336)	1336	1335	+
U/C ring stretching (1460)	1460	1458	-
A/G ring stretching (1485)	1480	1478	+
A/G ring stretching (1578)	1576	1578	+

FIGURE LEGENDS

FIG. 1. The scheme used to purify EV1 produces homogenous population of intact virions. (A) Sucrose gradient fractioned from the top shows clear separation in optical density (OD260) between bulk, low-density material, and EV1 virions. Fractions 11, 12 and 13 were collected for further purification. (B) Absorption spectrum of Dialyzed EV1 (dashed line) and light scattering corrected spectrum (solid line) normalized at 260 nm for better comparison between the two. The

scattering component was calculated to be 6.9% of the total signal and 260/280 ratio was 1.65. (C) SDS-PAGE analysis of the purified EV1 samples shows no protein contaminants in the range of 250-10 kDa, while prominent viral proteins VP1-3 band between 35 kDa and 25 kDa markers. (D) EV1 particles contrasted by negative staining and visualized by TEM show homogenous population of intact virions approx 25 nm in diameter. Scale bar is 100 nm.

FIG. 2. Thermal stability analysis of intact EV1 virions. (A) Fluorescence traces of SYBR Green II in the presence of EV1 show steep increase starting from around 40°C and a midpoint at 51°C (solid line). The SYBR Green II by itself shows no fluorescence increase as a function of temperature (dashed line). The fluorescence is normalized with respect to the initial fluorescence. (B) EV1 was incubated with SYBR Green II at 50°C and 60°C for 3 and 10 minutes, respectively, and cooled back to 20°C for fluorescence measurement. At 20°C EV1 is not permeable to the dye, whereas temperature induced genome egress is detected as an increase in fluorescence. White bar represent the behavior of SYBR Green II alone when subjected to the described treatment.

FIG. 3. TEM images of negative stained EV1. (A) Intact EV1 virion. (B) EV1 heated at 50°C for 3 minutes show protruding density from an otherwise structured particle. (C) Heating for 10 minutes at 60°C result in complete particle disruption. Scale bars are 25 nm and 100 nm for the left hand side and right hand side images, respectively.

FIG. 4. Comparison of the Raman spectra of dried and aqueous EV1 particles. (A)

855 The full Raman spectra of dried intact EV1 virion. The most prominent vibrational
856 region is the aliphatic C-H stretching complex shown at around 2900 cm^{-1} which,
857 however, has a low information content of the structural details of the virion particles.
858 The fingerprint region locates between 700 and 1800 cm^{-1}. The sharp band at 2331
859 cm^{-1} originates from N_2. (B) The fingerprint region of dried EV1 virion (top line) and
860 aqueous EV1 at 0.9 mg ml^{-1} and 3.8 mg ml^{-1} concentrations (middle and bottom
861 lines, respectively). Laser excitation with 532 nm and powers of 45 mW for dried and
862 200 mW for the aqueous viral samples were used with 30 exposures of 10 s in each
863 measurement. The spectra were normalized to the Phe vibration at 1003 cm^{-1} and
864 the baseline was shifted for better comparison of the spectra. All spectra were
865 measured at ambient temperature.
866
867 **FIG. 5.** The Raman spectra of aqueous EV1 particles at room temperature. On top,
868 the Raman spectra of intact EV1 (RT, black line), intermediate particles (50°C, blue
869 line) and disrupted particles (60°C, red line) are presented. Below, are the twofold
870 magnified difference spectra corresponding to the temperature intervals 60°C-RT
871 (red) and 50°C-RT (blue). The spectra are divided to individual sections and
872 normalized to mean signals of each section and the baselines were shifted for better
873 visualization. (A) 610-945 cm^{-1} (B) 945-1245 cm^{-1} (C) 1245-1520 cm^{-1}, and (D) 1520-
874 1800 cm^{-1}. Marked vibrations from lower to higher frequency: 726 cm^{-1}, RNA; 783
875 cm^{-1}, RNA; 811 cm^{-1}, RNA phosphate symmetric stretching, an A form RNA helix
876 marker; 1003 cm^{-1}, Phe; 1096 cm^{-1}, a complex region of CC and CH vibrations of
877 lipid, RNA and protein capsid; 1127 cm^{-1}, non-aromatic amino acids and lipids; 1240
878 cm^{-1}, Am III; 1335 cm^{-1}, RNA bases; 1446 cm^{-1}, C-H vibrations from the proteins;
879 1478 cm^{-1}, RNA bases; 1572 cm^{-1}, Trp/RNA; 1668 cm^{-1}, Am I revealing information

about the secondary structure of the proteins. The data acquisition was performed as described in Fig. 4, and the spectra represent mean signals of measurements from three different EV1 batches all with a concentration of about 3.8 mg ml^{-1}.

FIG. 6. Radial distribution of salt bridge donors in EV1 protomer. (A) Single protomer (colored) positioning with respect to the whole capsid (half capsid displayed). (B) The radial distribution of all atoms in EV1 protomer (PDB entry: 1EV1) are depicted in the grey histogram to illustrate the density of the capsid shell. In color, VP1 (blue), VP2 (red), VP3 (green) and VP4 (yellow), and the positioning of the salt bridge forming amino acids (Lys, Arg) in a single protomer, followed by their sequential positioning within these structural proteins. (C) The distribution of the salt bridge donors shows varying degree of connectivity within and between protomers. Interestingly, inner protein VP4 is mainly forming connections between protomers and one inner VP-VP connection.

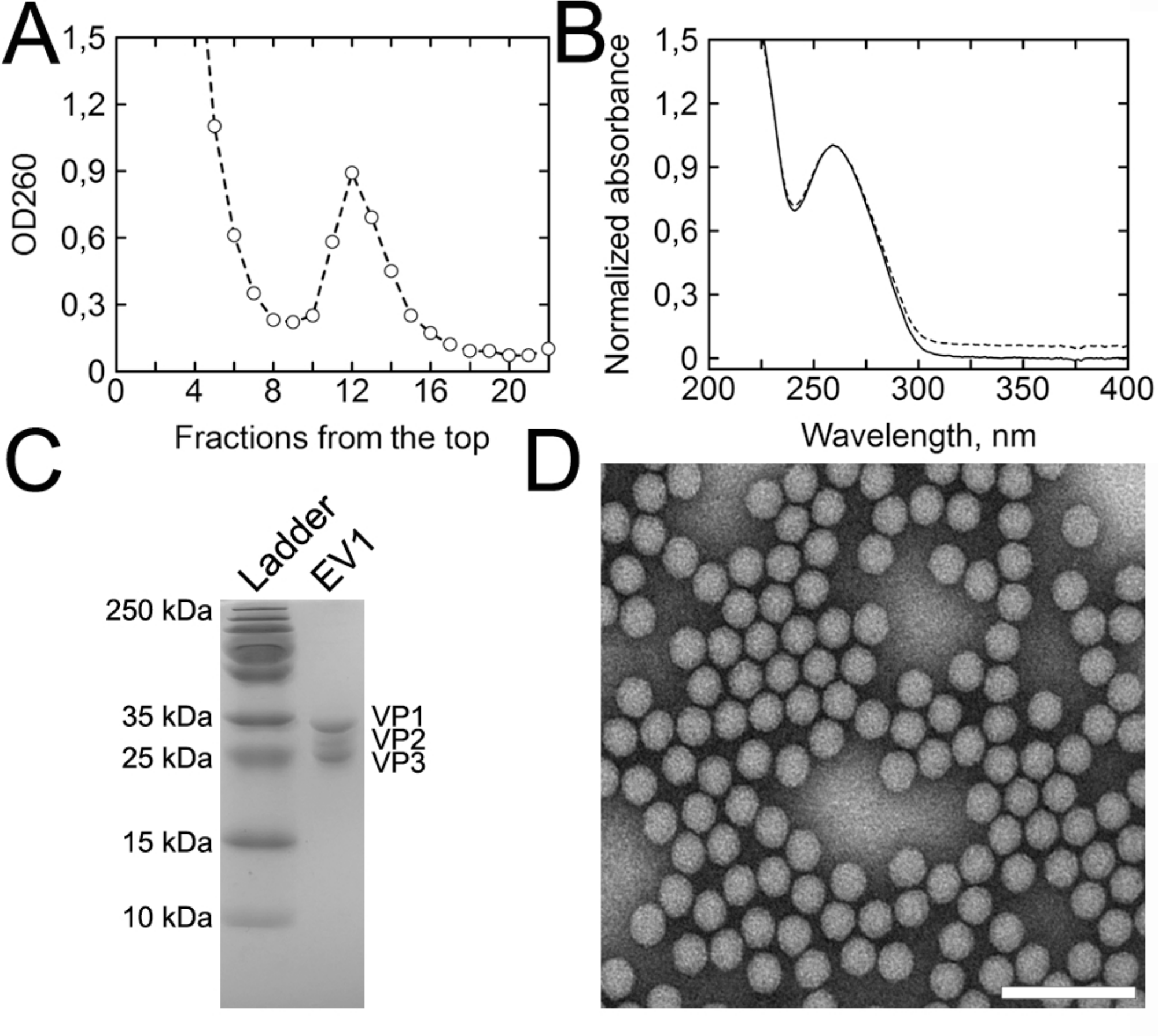
A
OD260
1,5
1,2
0,9
0,6
0,3
0
0
4
8
12
16
20
Fractions from the top
B
Normalized absorbance
1,5
1,2
0,9
0,6
0,3
0
200
250
300
350
400
Wavelength, nm
C
Ladder
EV1
250 kDa
35 kDa
25 kDa
15 kDa
10 kDa
VP1
VP2
VP3
D

A

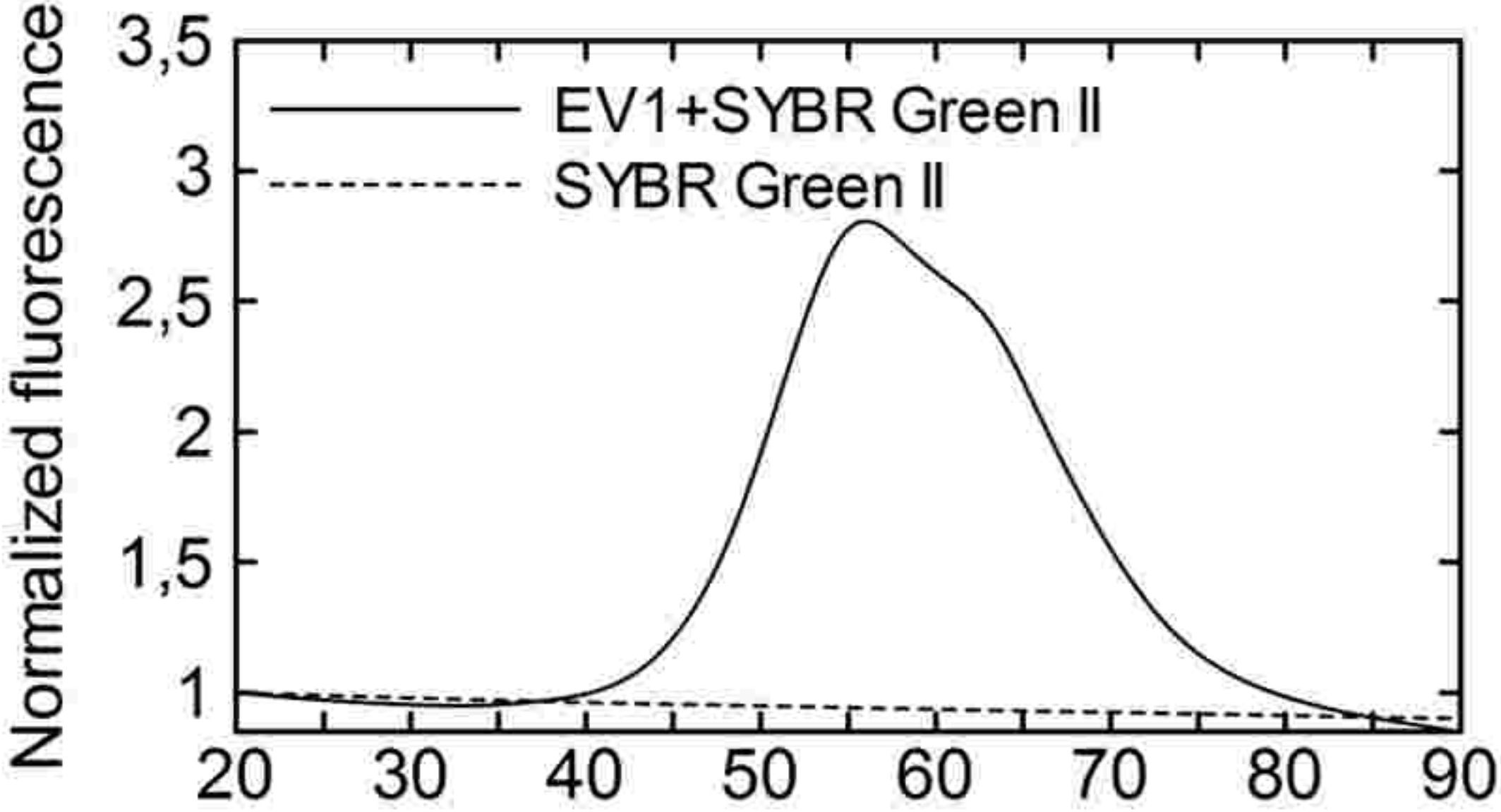
Normalized fluorescence
3,5
3
2,5
2
1,5
1
EV1+SYBR Green II
SYBR Green II
20
30
40
50
60
70
80
90
Temperature, °C

B

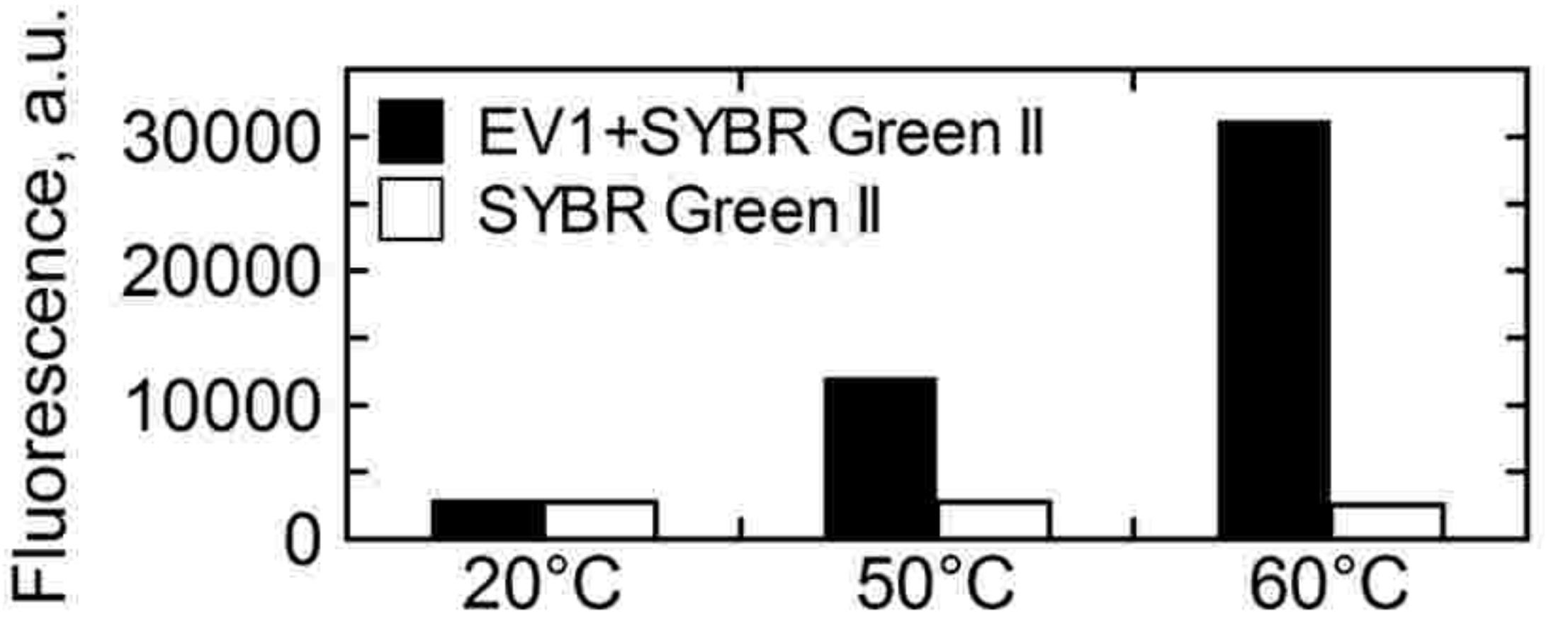
Fluorescence, a.u.
30000
20000
10000
0
EV1+SYBR Green II
SYBR Green II
20°C
50°C
60°C

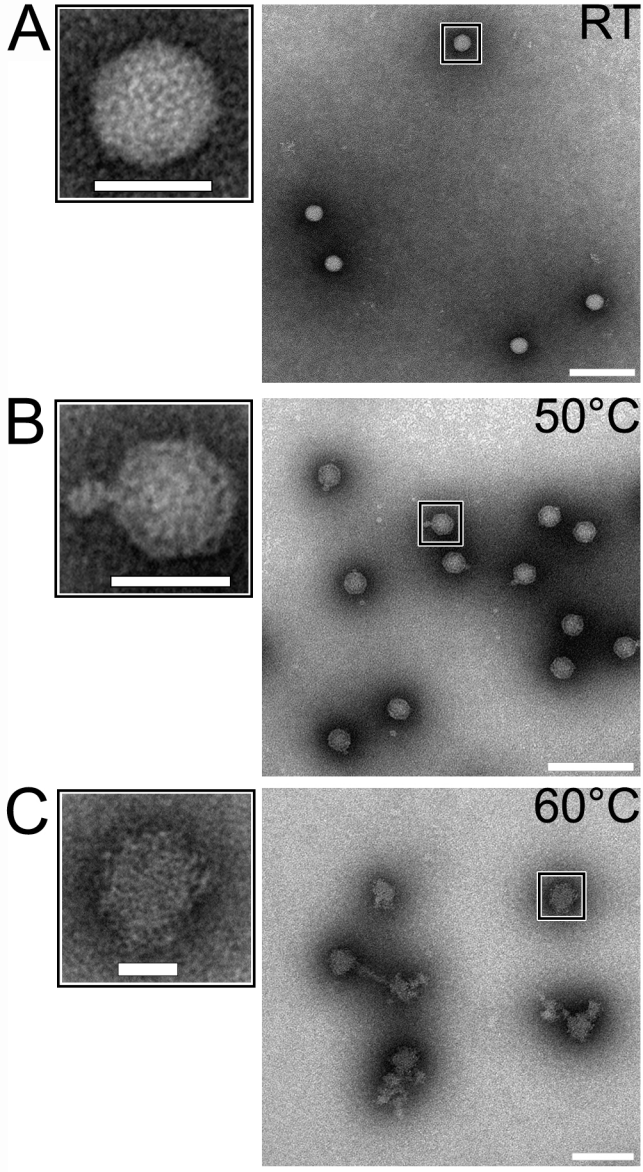
A
RT
B
50°C
C
60°C

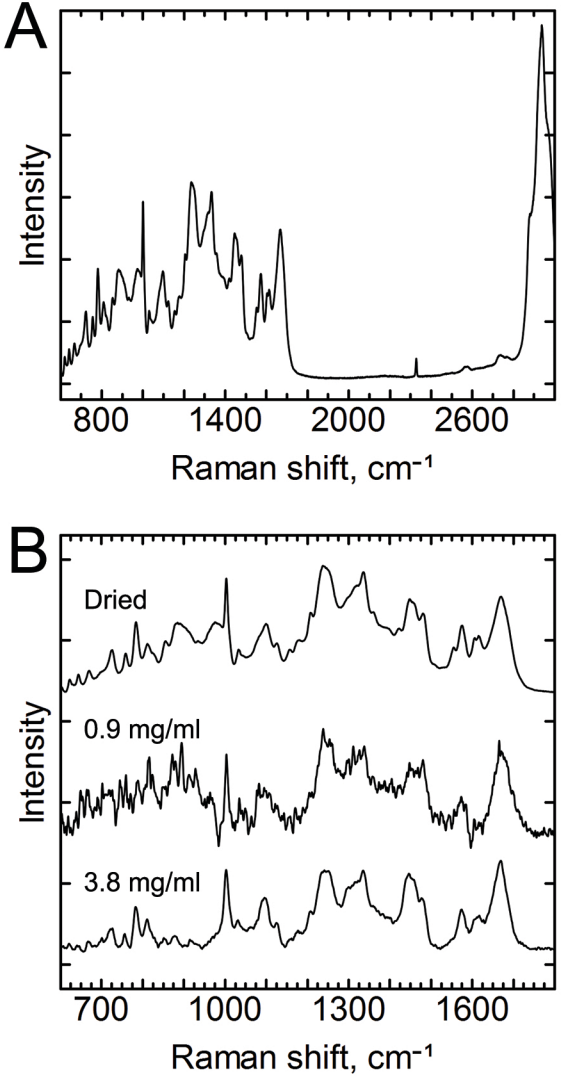
A
Intensity
800
1400
2000
2600
Raman shift, cm⁻¹
B
Dried
0.9 mg/ml
3.8 mg/ml
Intensity
700
1000
1300
1600
Raman shift, cm⁻¹

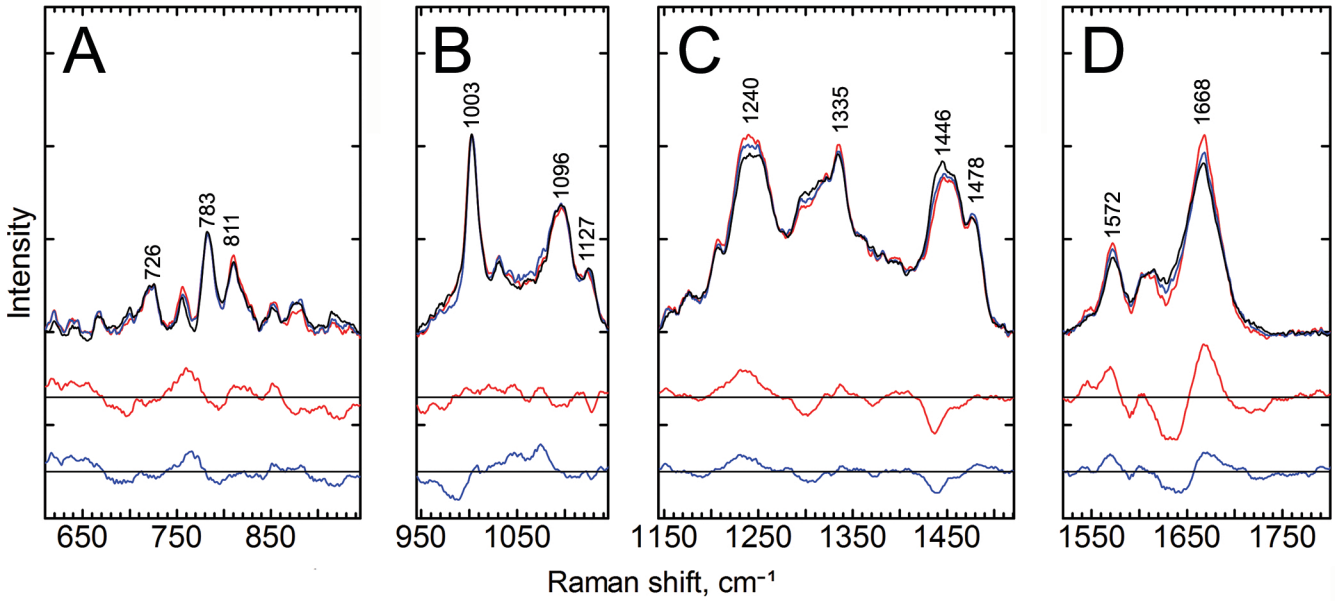
A
B
C
D
Intensity
726
783
811
1003
1096
1127
1240
1335
1446
1478
1572
1668
650
750
850
950
1050
1150
1250
1350
1450
1550
1650
1750
Raman shift, cm⁻¹

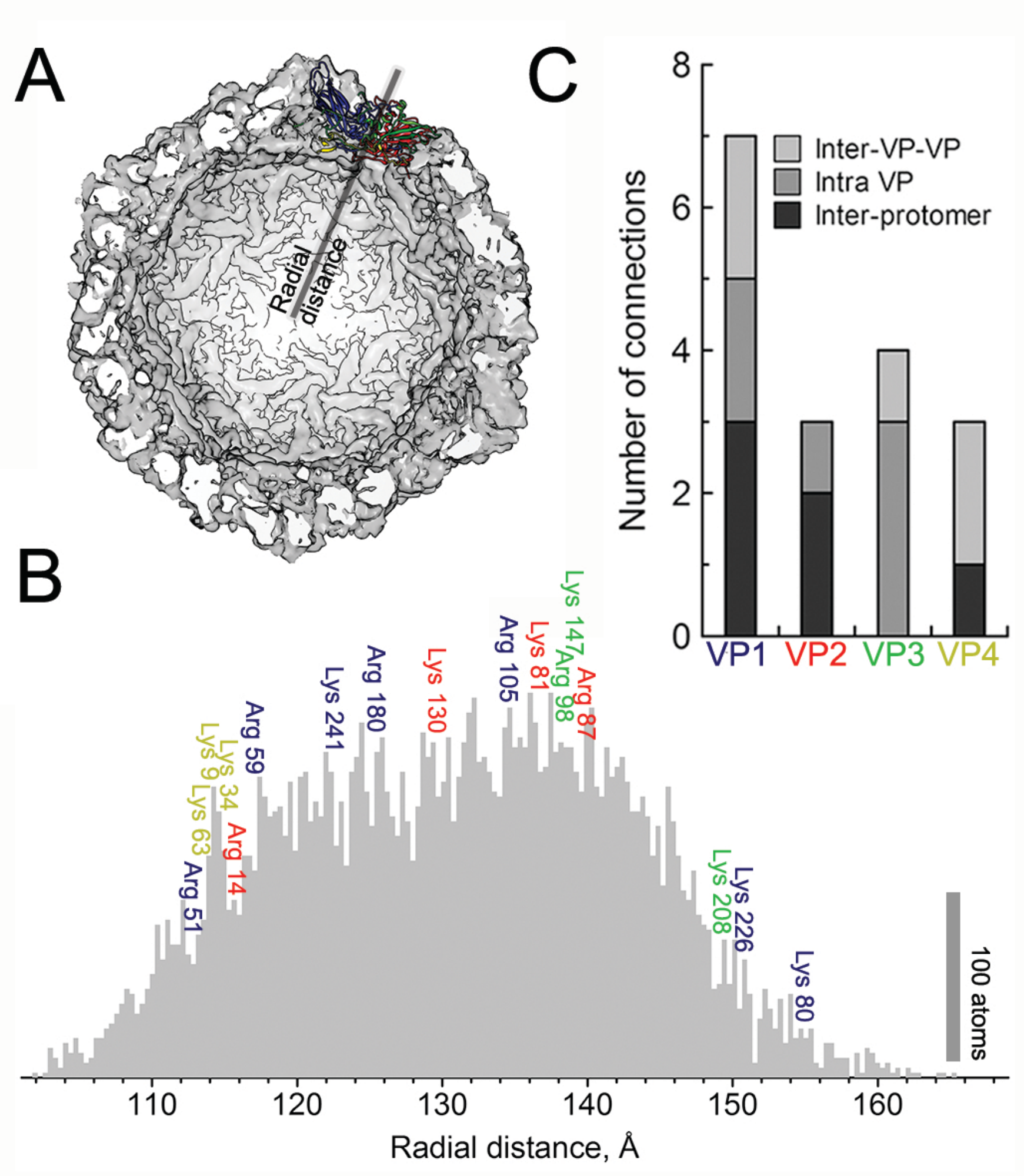
A
Radial distance
B
Lys 147
Arg 98
Arg 87
Lys 81
Arg 105
Lys 130
Arg 180
Lys 241
Arg 59
Lys 34
Lys 9
Lys 63
Arg 14
Arg 51
Lys 226
Lys 208
Lys 80
100 atoms
110
120
130
140
150
160
Radial distance, Å
C
Number of connections
0
2
4
6
8
Inter-VP-VP
Intra VP
Inter-protomer
VP1
VP2
VP3
VP4